Journal Pre-proof

Engineering of Silicone-based Mixtures for the Digital Light Processing of Åkermanite Scaffolds

Arish Dasan, Hamada Elsayed, Jozef Kraxner, Dušan Galusek, Paolo Colombo, Enrico Bernardo

PII: S0955-2219(19)30843-X

DOI: https://doi.org/10.1016/j.jeurceramsoc.2019.11.087

Reference: JECS 12912

To appear in: *Journal of the European Ceramic Society*

Received Date: 27 August 2019

Revised Date: 26 November 2019

Accepted Date: 29 November 2019

Please cite this article as: Dasan A, Elsayed H, Kraxner J, Galusek D, Colombo P, Bernardo E, Engineering of Silicone-based Mixtures for the Digital Light Processing of Åkermanite Scaffolds, *Journal of the European Ceramic Society* (2019), doi: https://doi.org/10.1016/j.jeurceramsoc.2019.11.087

Engineering of Silicone-based Mixtures for the Digital Light Processing of Åkermanite Scaffolds

Arish Dasan[a], Hamada Elsayed[b,c], Jozef Kraxner[a], Dušan Galusek[d], Paolo Colombo[c],[e] Enrico Bernardo[c*]

[a] Department of Glass Processing, FunGlass, Alexander Dubček University of Trenčín, Trenčín, Slovakia

[b] Ceramics Department, National Research Centre, Cairo, Egypt

[c] Department of Industrial Engineering, Università degli Studi di Padova, Padova, Italy

[d] Joint glass centre of the IIC SAS, TnUAD, and FChFT STU, FunGlass, Alexander Dubček University of Trenčín, Trenčín, Slovakia

[e] Department of Materials Science and Engineering, The Pennsylvania State University, University Park, PA 16802, USA

*Correspondence should be addressed: e-mail enrico.bernardo@unipd.it; fax +39 049 8275505

Abstract

Silicones mixed with oxide fillers are interesting precursors for several bioactive glass-ceramics. A key point is represented by the coupling of synthesis and shaping, since highly porous bodies, in form of foams or scaffolds, are first manufactured with silicones in the polymeric state, at low temperature, and later subjected to ceramic transformation. After successful application of direct ink writing, the present study illustrates the tuning of silicone-based mixtures in order to form åkermanite ($Ca_2MgSi_2O_7$) reticulated scaffolds by digital light processing. This implied the selection of commercial silicones, producing stable and homogeneous blends with a photocurable resin and enabling the manufacturing of defect-free printed scaffolds, before and after firing, without fillers. The blends were further refined with the introduction of fillers, followed by firing at 1100 °C, in air. Optimized samples (from H44 resin) and reactive fillers (including up to 4.5 wt.% borax additive), led to crack-free and phase-pure scaffolds with microporous struts.

Keywords

Åkermanite; 3D scaffolds; Polymer-derived Ceramics; Additive Manufacturing; Digital Light Processing

1. Introduction

Silicone resins filled with oxide fillers, when fired in air, generally offer the possibility to develop crystalline silicate or alumino-silicate ceramics of wide engineering interest (mullite, forsterite, zircon, cordierite, gehlenite, etc.) in conditions of high phase purity and low processing temperature [1, 2]. Similarly to un-filled preceramic polymers [3], a distinctive feature consists of the coupling of synthesis and shaping, since some components may be first manufactured using silicones still in the polymeric state and then transformed into crack-free ceramics by firing.

The high flexibility in the design of components has been exploited mainly for Ca-based silicates, produced in the form of highly porous foams and scaffolds, to be used for bone tissue applications [4], [5]. Additive manufacturing technologies are often applied [6]-[7], [8]. In this framework, attention is paid also to semi-crystalline materials, i.e. glass-ceramics, with fillers controlling the chemistry of both crystals and the surrounding glass phase. As an example, silicones (providing SiO_2) filled with calcium carbonate, sodium carbonate and sodium phosphate (providing CaO, Na_2O and P_2O_5, respectively) have been recently used for obtaining porous glass-ceramics, by direct firing at 1000 °C, with chemical and mineralogical compositions exactly matching those of Biosilicate® glass-ceramics (belonging to the Na_2O-CaO-SiO_2-P_2O_5 system) produced from conventional processing [**Error! Bookmark not defined.**].

Borates and phosphates (including sodium phosphate, in the formulation of polymer-derived Biosilicate ® glass-ceramics) are recognized to act as 'multifunctional' fillers. In hydrated form, they contribute to the shaping of highly porous samples [9],[10], by causing water vapour release within silicone matrices at the early stages of heat treatment, i.e. still in the polymeric state (the dehydration occurs at only 300-350 °C). At higher temperatures, in any form (hydrated or not), they develop some liquid phase, favoring the synthesis of the desired silicate phases, by enhancing the ionic interdiffusion, and releasing internal stresses, due to gas evolution upon conversion of silicones into ceramics. This liquid phase generates most of the glass matrix upon cooling. Minor amounts of CaO, MgO, SiO_2, etc., expected to be present only in the crystal phases, stay dissolved in the glass phase [**Error! Bookmark not defined.**]. The additives are finally expected to improve the polymer-derived biomaterials, by offering extra functionalities, as shown by Balasubramanian et al., concerning boron inclusion in silicates [11]).

The present paper deals with the tuning of silicone-based mixtures, aimed at developing åkermanite ($Ca_2MgSi_2O_7$) bioceramic scaffolds by means of advanced additive manufacturing, such as stereolithography, that enable the fabrication of samples with very complex shapes. Again, the key point is represented by the coupling of synthesis and shaping, since stereolithography was not applied on mixtures of a sacrificial photocurable acrylate resin and pre-synthesized glass particles, as in recent experiences on bioactive glass-ceramics [12], but on engineered photocurable blends. The specific system (Ca-Mg silicate) is known for its potential for bone tissue engineering, due to the excellent bioactivity and biocompatibility, observed also for polymer-derived foams [13].

Preceramic polymers, i.e. polymers undergoing transformation by thermal treatment into (mainly Si-based) advanced ceramics [**Error! Bookmark not defined.**], offer by themselves distinctive advantages in

the shaping by means of lithographic methods [14], [15]. In particular, advanced reticulated structures can be obtained by stereolithography [16]. Photocurable slurries, i.e. biphasic mixtures, consisting of photocurable liquid and suspended ceramic powders, may be replaced by a photocurable preceramic polymer, commercially available [17]-[18],[19] or developed by chemical modification of a non-photocurable preceramic polymer [20]-, [21], [22]. The inherent homogeneity (due to the absence of suspended powders, of any size) favours an extremely high resolution. Although leading to extraordinary materials, stereolithography of preceramic polymers has some constraints in the chemistry of the resulting ceramic material, since it leads to the development of silicon oxycarbide ceramics (SiOC) [**Error! Bookmark not defined.**,**Error! Bookmark not defined.**], still not fully recognized as suitable biomaterials per se [23]-[24], [25], [26], . In addition, we cannot exclude the presence of heavy metal traces [27], used as catalysts, that would impair the biological applications.

In the present study we extend the application of stereolithography to filled silicones, previously tested for mullite ceramics [28], to blends based on a sacrificial photocurable resin mixed with three non-photocurable silicones, already known for yielding biocompatible and bioactive glass-ceramics [9, [29]. After the selection of the best silicone (H44 resin), by means of tests on the manufacturing of pure SiOC scaffolds, the addition of reactive fillers (including up to 4.5 wt.% of borax additive) effectively led to crack-free, phase-pure åkermanite bioceramic scaffolds, with microporous struts.

2. Experimental procedure

The preceramic polymers used in this study consisted of commercially available silicones (Wacker-Chemie GmbH, Munich, Germany) in powder (H44 type) and liquid (H62C) form. These silicones were blended with a commercial photocurable liquid acrylate (acrylate monomers and glycol diacrylate monomers mixed with phosphine oxide based photo initiator, Standard Blend (SB), Fun To Do, Alkmaar, The Netherlands). Initial experiments involved just the mixing of the liquid acrylate with silicone solutions in isopropyl alcohol (Sigma Aldrich, Gillingham, UK), forming mixtures corresponding to the silicone/solvent/SB weight proportions of 1/0.3/1. The mixing was performed using a planetary mixer (THINKY ARE-250), for 30 min, at a speed of 2000 rpm./min.

Homogeneous mixtures were processed by means of a DLP printer (3DLPrinter-HD 2.0, Robotfactory S.r.l., Mirano, Italy) operating in the visible light range (400–500 nm). The layer thickness was set at 50 μm with an exposure time of 3 s. The specific energy dose was approximately 7.43 mJ cm^{-2} (as communicated by manufacturers of the DLP equipment, computed according tothe exposure time, the average light power, and sensor spot size).. After printing, the structures were cleaned by sonication in diphenylether (Sigma Aldrich, Gillingham, UK) bath and by flow of compressed air. To ensure complete hardening, the printed parts were further cured in an UV chamber (365 nm, Robotfactory S.r.l., Mirano, Italy), for 15 min. Finally, the printed parts were transformed to ceramic by controlled heat treatment under nitrogen atmosphere in two steps (550 °C for 3 h with a heating rate of 0.5 °C/min; 1000 °C for 1 h with a heating rate of 2 °C/min), followed by natural cooling.

Åkermanite ceramics were developed by by introduction of selected fillers such as $CaCO_3$ and $Mg(OH)_2$ micro-powders (<10 μm, Industrie Bitossi, Vinci, Italy), nano-sized MgO (30 nm, Inframat Advanced Materials, Manchester, CT, USA) and borax, in both anhydrous ($Na_2B_4O_7$) and hydrated ($Na_2B_4O_7 \cdot 10H_2O$) form (Sigma Aldrich, Gillingham, UK), in SB/silicone blends. The printed green bodies were fired in air with different stepwise heat treatment: 80 °C/5 h, 200 °C/1 h, 550 °C/3 h, 650 °C/1 h, 800 °C/3 h and finally 1100 °C/3 h. In order to avoid crack formation, due to evaporation and burn-out of organic components, the heating rate was fixed at 0.2 °C/min, up to 650 °C, followed by 0.5 °C/min.

Microstructural characterizations on the fired scaffolds were conducted by optical stereomicroscopy (AxioCamERc 5s Microscope Camera, Carl Zeiss Microscopy, Thornwood, New York, USA) and scanning electron microscopy (FEI Quanta 200 ESEM, Eindhoven, Netherlands). The crystalline phases were identified by X-ray diffraction on powdered samples (XRD; Bruker AXS D8 Advance, Karlsruhe, Germany), supported by data from PDF-2 database (ICDD-International Centre for Diffraction Data, Newtown Square, PA) and the Match! program package (Crystal Impact GbR, Bonn, Germany).

The density of the ceramized scaffolds was measured geometrically using a digital caliper and by weighing with an analytical balance. The apparent and true densities of the printed parts were measured by pycnometer (Micromeritics AccuPyc 1330, Norcross, GA), operating with helium gas on samples in bulk (3D printed scaffold) and powder forms. The compressive strength of sintered scaffolds was evaluated at room temperature, using an Instron 1121 UTM (Instron Danvers, MA), at a crosshead speed of 0.5 mm/min. Each data point represents the average value of at least 10 individual tests.

3. Results and discussion

3.1 Un-filled SB/silicone blends

Preliminary tests involved the use of MK methyl-silicone (Wacker-Chemie GmbH, Munich, Germany), which was the reference materials employed previously for the fabrication by direct ink writing of polymer-derived Biosilicate® and åkermanite scaffolds [**Error! Bookmark not defined.**,**Error! Bookmark not defined.**]. MK provides a higher SiO_2 yield upon pyrolysis in air (84 wt.%), compared with H44 (52.5 wt.%) and H62C (58 wt.%) [**Error! Bookmark not defined.**,**Error! Bookmark not defined.**]. However, the mixing with SB was difficult. In fact, MK based blends tended to phase-separate within 30 min and the highly sticky nature of the mixture impeded the obtainment of any well-defined shape upon printing.

On the contrary, H44 and H62C methyl-phenyl-silicone resins gave stable mixtures with SB, which were easily processable by DLP. In particular, H44 powders could be added to SB even without solvent. This is evident from Fig. 1, showing H44-derived samples after firing at 1000 °C in N_2: despite considerable linear volume shrinkage (42±1%), the samples did not present any cracks or defects. Cubic-cell samples exhibited a very good finish (Figs. 1a,b); higher magnification details (Fig. 1c) reveal some uniform surface features, deriving from the post-printing cleaning procedure and the limited presence of some pores (dark spots), deriving from the decomposition of the organics in the mixture. Samples with a diamond cell architecture exhibited the typical stair-stepping effect of DLP (Fig. 1d), indicating that the thermal curing of

silicone resin, coupled with the presence of the acrylic rein, was sufficient to prevent flow of the material when heated above its glass transition temperature.

FIGURE 1 HERE

Fig. 1 – Details of scaffolds from H44-photocurable acrylic resin blend, fired in nitrogen: a-c) cubic-cell sample; c,d) diamond-cell sample

Samples prepared from H62C, when examined by optical microscope (not shown), appeared quite similar to those prepared from H44 (Figs. 1a,b). High magnification details (Fig. 2), however, revealed lower homogeneity, probably due to non-uniform dispersion of the silicone in the photocurable liquid: the surface finish of cubic-cell samples was not satisfactory (Fig. 2a) and featured compact regions embedded in a porous matrix (Fig .2b). Diamond-cell scaffolds (Fig. 2c) did not keep a neat stair-stepping effect, possibly due to a lower thermal crosslinking efficiency for this silicone resin in comparison to the H44 resin, leading to some viscous flow.

FIGURE 2 HERE

Fig. 2 - Details of scaffolds from H62C-photocurable acrylic resin blend, fired in nitrogen: a,b) cubic-cell sample; c) diamond-cell scaffold

A small reduction in the mechanical properties of SiOC scaffolds from H62C, compared to those from H44, was observed (Table 1), compatible with the mentioned differences in microstructure. With the same cubic-cell morphology, SiOC scaffolds exhibited nearly the same geometrical density, the same distribution between open and closed porosity (closed porosity being only ~4.5 vol.% of the total), and a similar compressive strength (exceeding 20 MPa). Passing to a diamond cell structure implied an overall reduction of geometrical density and a reduction of the closed porosity (~2.5 vol.% of the total). The observed compressive strength (2-3 MPa) is far from being low, given the high value for the total porosity. According to the well-known Gibson&Ashby model for the scaling of compressive strength (σ_c) with relative density (ρ_{rel}) in open-celled bending-dominated structures ($\sigma_c \cong 0.2 \cdot \sigma_{bend} \cdot (\rho_{rel})^{1.5}$ [30]), we estimated a bending strength of the solid phase (σ_{bend}) not below 200 MPa, far above that of silicate glasses [31]. We did not apply the analysis to cubic-cell samples, considering the presence of relatively thick struts.

TABLE 1 HERE

Table 1 - Physical and mechanical properties of SiOC scaffolds

3.2 Åkermanite-based 3D scaffolds

The addition of fillers determined additional processing complications. The transformation of many silicones into SiOC, upon the firing in N_2, is still unclear in terms of exact quantification of the Si/O/C atomic balance. H44 represents an exemption, with the deriving SiOC known to correspond to the chemical formula $Si_3O_{4.6}C_{8.45}$ [32]. However, it should be observed that the inclusion of fillers influences the formulation of polymer-derived SiOC, as previously observed with wollastonite-diopside foams [**Error! Bookmark not defined.**]. The firing in air was thus applied to simplify the ceramic conversion of silicones, into pure silica, according to above mentioned ceramic yields (52.5 wt.% for H44, 58 wt.% for H62C). An

increase of the firing temperature, up to 1100 °C, was adopted in order to maximize the interdiffusion through the liquid phase, in turn provided by anhydrous borax, initially set at 1.5 wt.% of the total ceramic yield of the other components [**Error! Bookmark not defined.**].

Fig. 4 clearly demonstrates the higher suitability of H44 as a precursor for the target crystalline phase, with diffraction peaks matching those of the desired phase ($Ca_2MgSi_2O_7$, PDF#87-0049). Only traces of wollastonite (β-$CaSiO_3$, PDF#76-0925) were detected as a minor crystalline phase. The sample from H62C, on the contrary, featured substantial signals attributed to merwinite ($Ca_3MgSi_2O_8$, PDF#89-2432) - i.e. to a Ca-Mg silicate with different $CaO/MgO/SiO_2$ balance -, to unreacted MgO (periclase, PDF#89-4248) and to crystalline SiO_2 (cristobalite, PDF#82-1014). The inhomogeneity already observed without fillers, upon firing in nitrogen, evidently resulted in inhomogenous reactions between the polymer-derived silica and fillers.

FIGURE 3 HERE

Fig. 3 – Mineralogical comparison of samples from silicone-photocurable acrylic resin-reactive fillers blends, fired in air (at 1100 °C), based on: a) H62C; b) H44

FIGURE 4 HERE

Fig. 4 – Microstructural details of samples containing anhydrous borax (1.5 wt.% $Na_2B_4O_7$ addition): a) macro-cracks in cubic-cell scaffold; b) defect within a strut of a diamond-cell scaffold; c) microporous structure of struts

The samples from H44, despite the excellent phase assemblage, still had some drawbacks. As shown by Fig. 4a, the scaffolds contained many macro-cracks. Their strength was insufficient, so they could break under gentle hand pressure. Anhydrous fillers (MgO and $Na_2B_4O_7$), firstly selected, were expected to minimize the gas evolution upon ceramic conversion; however, this choice led to some agglomerates, likely due to the hygroscopicity of the same fillers, in turn causing the cracking. Fig. 4b, as an example, illustrates a large defect in the cross-section of the strut of a diamond-cell sample. Interestingly, higher magnifications of the same cross-section, as shown by Fig. 4c, revealed a spongy, foamed structure. The multitude of pores could be attributed to gas release from the decomposition of $CaCO_3$ filler and SB/H44 blend.

Based on the microstructural observations, we can conclude that preceramic polymers and reactive fillers were confirmed to enable the fabrication of scaffolds with hierarchical porosity also by digital light processing, after successful experiments with scaffolds produced by direct ink writing of silicone-based pastes [**Error! Bookmark not defined.**]. Such scaffolds possessing hierarchical porosity represent a significant research target in recent bioceramics (sometimes achieved by quite complex processing, such as the printing of emulsions instead of ceramic pastes [33], [34], [35] , in order to combine cell attachment, growth and differentiation, infiltration of body fluids and vascularization [36],[37].

More homogeneous blends were achieved when using hydrated fillers. As shown in Fig. 5a, macrocracks were still present, at low borax addition (1.5 wt.%). A good homogeneity was indirectly indicated by the diffraction pattern in Fig. 6: despite involving a micro-sized MgO precursor, the new blend provided nearly phase pure åkermanite, as in the previous case with nano-sized MgO. Increasing the borax

addition reduced or eliminated both the formation of microcracks (Figs. 5b,c) and the presence of wollastonite secondary phase (Fig. 6).

FIGURE 5 HERE

Fig. 5 – Microstructural details of cubic-cell scaffolds from hydrated borax (a: 1.5 wt.% $Na_2B_4O_7$ addition; b: 3 wt.%; c: 4.5 wt.%)

FIGURE 6 HERE

Fig. 6 – Mineralogical analysis of scaffolds fired at 1100 °C from H44-based mixture added with hydrated borax: (a: 1.5 wt.% $Na_2B_4O_7$ addition; b: 3 wt.%; c: 4.5 wt.%)

The spongy, foamed structure of the struts was confirmed also in the case of hydrated fillers, as shown in Fig. 7. Quite surprisingly, there was no extra foaming effect from the release of water vapour, the microporous struts from hydrated fillers (1.5-3 wt.%, Figs. 7a,b) being quite similar to those formed with anhydrous fillers (Fig. 4c). In the previous investigation on scaffolds from MK-derived pastes printed by direct ink writing, passing from anhydrous to hydrated filler determined a clearly visible transition from nearly fully dense to foamed struts [**Error! Bookmark not defined.**]. MK silicone evidently had not undergone a substantial cross-linking, at low temperature, so that water vapour release (at 300-350 °C, due to the decomposition of both Mg hydroxide and borax), could occur in a viscous matrix. The acrylate resin/silicone blend used for DLP experiments reasonably led to a highly cross-linked matrix, not undergoing any softening at the early stage of heat treatment.

The maximum amount of borax (for a $Na_2B_4O_7$ addition of 4.5 wt.%) had an interesting microstructural effect, with micropores surrounding interlocking elongated åkermanite crystals, as shown by Fig. 7c. This is in agreement with previous experiments with foams [**Error! Bookmark not defined.**]; a more abundant liquid phase surrounding the reactants (polymer-derived SiO_2, CaO and MgO), evidently favored anisotropic crystal growth (a similar condition is known for mullite crystals in clay-derived vitreous ceramics, presenting a more acicular morphology in more fluxed, and more fluid, matrices [38]).

FIGURE 7 HERE

Fig. 7 – Microstructural details of H44-derived diamond-cell samples: a) 1.5 wt.% $Na_2B_4O_7$ addition; b) 3 wt.%; c,d) 4.5 wt.%)

Table 2 reports data from physical and mechanical characterizations of the H44-based scaffolds involving reactive fillers. Both total and open porosity increased significantly, compared to scaffolds from the blend not comprising reactive fillers and fired in N_2, as an effect of the formation of highly porous struts. As an example, with 1.5 wt.% $Na_2B_4O_7$ addition, the total porosity of the cubic-cell scaffold passed from 62 to 74 vol.%. The almost non-existing closed porosity indicate the full gas permeability of the structure.

Increased amounts of borate salt reduced total porosity (from 74 to 66 vol.%), due to enhancement of viscous flow. In any case, the porosity remained mostly open. The observed compressive strength values (from 1.5 to 2.8 MPa) remained within the range generally exhibited by silicate scaffolds for bone tissue engineering, with the same level of porosity [39].

Changing the design from cubic to diamond cells did not imply any cracking, as confirmed by Fig. 7d, but caused a significant reduction of compressive strength. Again, this must be seen in the light of the increased porosity, approaching 90 vol.%. Applying the above-mentioned Gibson&Ashby model, we could estimate a bending strength of ~50 MPa, well below the strength values of glass-ceramics; the model, however, neglects any stress concentration effect, arising from the porosity in the struts. Anyway, the compressive strength of the sample with 4.5 wt.% $Na_2B_4O_7$ addition still compares well with the values for silicate scaffolds with the same porosity [**Error! Bookmark not defined.**]. Additional efforts will be carried out, in the near future, to improve the strength by revision of the designs. Finally, extensive cell studies are envisaged to confirm the high biocompatibility and bioactivity expected from åkermanite-based ceramics.

TABLE 2 HERE

Table 2 - Physical and mechanical properties of åkermanite scaffolds from H44-based mixtures

Conclusions

Based on the presented results the following conclusions can be drawn:

- Åkermanite scaffolds, with hierarchical porosity, were easily manufactured by digital light processing of silicone-based photocurable mixtures;
- Silicone/acrylate resin blends could be used instead of photocurable silicones; the high homogeneity could be exploited both for the manufacturing of SiOC ceramics, without fillers, and for the manufacturing of multicomponent silicate ceramics, including reactive oxide fillers;
- The microporosity of the struts was not determined by water release from hydrated fillers, but from the decomposition of $CaCO_3$ filler and SB/H44 blend;
- Hydrated fillers favored the development of homogeneous blends, in turn leading to defect free scaffolds.

Acknowledgements

The research was funded by the European Union's Horizon 2020 research and innovation programme under the H2020-WIDESPREAD-01-2016-2017-TeamingPhase2 project FunGlass (Centre for Functional and Surface Functionalized Glass), grant agreement No. 739566. Discussions with Prof. A. R. Boccaccini (University of Erlangen-Nuremberg, Germany), scientific board member (Biomaterials) of the Centre for Functional and Surface Functionalized Glass, are gratefully acknowledged.

References

[1]. P. Colombo, E. Bernardo, G. Parcianello, Multifunctional advanced ceramics from preceramic polymers and nano-sized active fillers, J. Eur. Ceram. Soc. 33 (2013) 453-469. https://doi.org/10.1016/j.jeurceramsoc.2012.10.006.

[2]. E. Bernardo, L. Fiocco, G. Parcianello, E. Storti, P. Colombo, Advanced ceramics from preceramic polymers modified at the nano-Scale: A review, Materials 7 (2014) 1927-1956. https://doi.org/10.3390/ma7031927.

[3] P. Colombo, G. Mera, R. Riedel, G.D. Sorarù, Polymer-Derived-Ceramics: 40 years of research and innovation in advanced ceramics, J. Am. Ceram. Soc. 93 (2010) 1805–1837. https://doi.org/10.1111/j.1551-2916.2010.03876.x.

[4] C. Wu, J. Chang, A review of bioactive silicate ceramics, Biomed. Mater. 8 (2013) 032001-12. Doi:10.1088/1748-6041/8/3/032001.

[5] Y. Huang, C. Wu, X. Zhang, J. Chang, K. Dai, Regulation of immune response by bioactive ions released from silicate bioceramics for bone regeneration, Acta Biomater. 66 (2018) 81–92. https://doi.org/10.1016/j.actbio.2017.08.044.

[6]. H. Elsayed, C. Gardin, L. Ferroni, B. Zavan, P. Colombo, E. Bernardo, Highly porous Sr/Mg-doped hardystonite bioceramics from preceramic polymers and reactive fillers: Direct foaming and direct ink writing, Adv. Eng. Mater. 21 (2019) 1800900. https://doi.org/10.1002/adem.201800900.

[7] H. Elsayed, P. Rebesan, M.C. Crovace, E. D. Zanotto, P. Colombo, E. Bernardo, Biosilicate® scaffolds produced by 3D printing and direct foaming using preceramic polymers, J. Am. Ceram. Soc. 102 (2019) 1010-1020. https://doi.org/10.1111/jace.15948.

[8]. A. Dasan, H. Elsayed, J. Kraxner, D. Galusek, E. Bernardo, Hierarchically porous 3D-printed akermanite scaffolds from silicones and engineered fillers, J. Eur. Ceram. Soc. 39 (2019) 4445-4449. https://doi.org/10.1016/j.jeurceramsoc.2019.06.021.

[9]. L. Fiocco, H. Elsayed, L. Ferroni, C. Gardin, B. Zavan, E. Bernardo, Bioactive Wollastonite-Diopside Foams from Preceramic Polymers and Reactive Oxide Fillers, Materials. 8 (2015) 2480-2494; https://doi.org/10.3390/ma8052480.

[10] E. Bernardo, J-F. Carlotti, P. Mendanha Dias, L. Fiocco, P. Colombo, L. Treccani, U. Hess, K. Rezwan, Novel akermanite-based bioceramics from preceramic polymers and oxide fillers, Ceram. Int. 40 (2014) 1029-1035. https://doi.org/10.1016/j.ceramint.2013.06.100.

[11] P. Balasubramanian, T. Büttner, V. Miguez Pacheco, A.R. Boccaccini, Boron-containing bioactive glasses in bone and soft tissue engineering, J. Eur. Ceram. Soc. 38 (2018) 855-869. https://doi.org/10.1016/j.jeurceramsoc.2017.11.001.

[12] J. Schmidt, H. Elsayed, E. Bernardo, P. Colombo, Digital light processing of wollastonite-diopside glass-ceramic complex structures, J. Eur. Ceram. Soc. 38 (2018) 4580-4584. https://doi.org/10.1016/j.jeurceramsoc.2018.06.004.

[13] L. Fiocco, S. Li, M.M. Stevens, E. Bernardo, J.R. Jones, Biocompatibility and bioactivity of porous polymer-derived Ca-Mg silicate ceramics, Acta Biomat. 50 (2017) 56–67. https://doi.org/10.1016/j.actbio.2016.12.043.

[14] M. Schulz, M. Börner, J. Haußelt, R. Heldele, Polymer derived ceramic microparts from X-ray lithography—cross-linking behavior and process optimization, J. Eur. Ceram. Soc. 25 (2005) 199-204. https://doi.org/10.1016/j.jeurceramsoc.2004.08.001.

[15] D-H. Lee, K-H. Park, L-Y. Hong, D-P. Kim, SiCN ceramic patterns fabricated by soft lithography techniques, Sensors and Actuators A: Physical. 135 (2007) 895-901. https://doi.org/10.1016/j.sna.2006.09.003.

[16] J. Schmidt, P. Colombo, Digital light processing of ceramic components from polysiloxanes, J. Eur. Ceram. Soc. 38 (2018) 57-66. https://doi.org/10.1016/j.jeurceramsoc.2017.07.033

[17]. L.-A. Liew, R.A. Saravanan, V.M. Bright, M.L. Dunn, J.W. Daily, R. Raj, Processing and characterization of silicon carbon-nitride ceramics: application of electrical properties towards MEMS thermal actuators, Sens. Actuators A: Phys. 103 (2003) 171-181. https://doi.org/10.1016/S0924-4247(02)00330-8.

[18]. T.-H. Yoon, S.-H. Park, K.-I. Min, X. Zhang, S.J. Haswell, D.-P. Kim, Novel inorganic polymer derived microreactors for organic microchemistry applications, Lab. Chip 8 (2008) 1454-1459. Doi: 10.1039/B804726J.

[19] S. Martínez-Crespiera, E. Ionescu, M. Schlosser, K. Flittner, G. Mistura, R. Riedel, H.F. Schlaak, Fabrication of silicon oxycarbide-based microcomponents via photolithographic and soft lithography approaches, Sens. Actuators A: Phys. 169 (2011) 242-249. https://doi.org/10.1016/j.sna.2011.04.041.

[20]. T.A. Pham, D.P. Kim, T.W. Lim, S.H. Park, D.Y. Yang, K.S. Lee, Three-dimensional SiCN ceramic microstructures via nano-stereolithography of inorganic polymer photoresists, Adv. Funct. Mater. 16 (2006) 1235-1241. https://doi.org/10.1002/adfm.200600009.

[21] Y.H. Li, X.D. Li, D.P. Kim, Chemical development of preceramic polyvinylsilazane photoresist for ceramic patterning, J. Electroceram. 23 (2009) 133-136. http://dx.doi.org/10.1007/s10832-007-9359-0.

[22]. E. Zanchetta, M. Cattaldo, G. Franchin, M. Schwentenwein, J. Homa, G. Brusatin, P. Colombo, Stereolithography of SiOC ceramic microcomponents, Adv. Mater. 28 (2016) 370-376. https://doi.org/10.1002/adma.201503470.

[23]. I. Gonzalo-Juan, R. Detsch, S. Mathur, E. Ionescu, A.R. Boccaccini, R. Riedel, Synthesis and in vitro activity assessment of novel silicon oxycarbide-based bioactive glasses, Materials. 9 (2016) 959. Doi:10.3390/ma9120959.

[24]. A. Francis, Progress in polymer-derived functional silicon-based ceramic composites for biomedical and engineering applications, Mater. Res. Express 5 (2018) 062003. Mater. Res. https://doi.org/10.1088/2053-1591/aacd28.
[25] E. Ionescu, S. Sen, G. Mera, A. Navrotsky, Structure, energetics and bioactivity of silicon oxycarbide-based amorphous ceramics with highly connected networks, J. Eur. Ceram. Soc. 38 (2018) 1311-1319. https://doi.org/10.1016/j.jeurceramsoc.2017.10.002.
[26]. M. Gawęda, P. Jeleń, E. Długoń, A. Wajda, M. Leśniak, W. Simka, M. Sowa, R. Detsch, A.R. Boccaccini, M. Sitarz, Bioactive layers based on black glasses on titanium substrates, J. Am. Ceram. Soc. 101 (2018) 590-601. https://doi.org/10.1111/jace.15202.
[27]https://www.tego-rc.com/product/break-thru/downloads/broc_tego-rc-practical-guide_en.pdf
[28]. J. Schmidt, A. Alpay Altun, M. Schwentenwein, P. Colombo, Complex mullite structures fabricated via digital light processing of a preceramic polysiloxane with active alumina fillers, J. Eur. Ceram. Soc. 39 (2019) 1336-1343. https://doi.org/10.1016/j.jeurceramsoc.2018.11.038.
[29] L. Fiocco, E. Bernardo, P. Colombo, I. Cacciotti, A. Bianco, D. Bellucci, A. Sola, V. Cannillo, Novel processing of bioglass ceramics from silicone resins containing micro- and nano-sized oxide particle fillers, J. Biomed. Mater. Res. A 102 (2014) 1549-3296. https://doi.org/10.1002/jbm.a.34918.
[30]. L.J. Gibson, M.G. Ashby, Cellular Solids, Structure and Properties. 2nd ed.; Cambridge University Press: Cambridge, UK, 1999.
[31] J.J. Swab, S.R. Thies, J.C. Wright, J.A. Schoenstein, P.J. Patel, Influence of surface scratches on the flexure strength of soda-lime silicate and borosilicate glass, Exp. Mech. 53 (2013) 91-96. Doi 10.1007/s11340-012-9674-5.
[32]. M. Scheffler, T. Takahashi, J. Kaschta, H. Muensted, P. Buhler, P. Greil, "Pyrolytic decomposition of preceramic organo polysiloxanes". In: Innovative Processing and Synthesis of Ceramics, Glasses, and Composites IV: Ceramic Transactions 115 (2000) 239-250.
[33]. C. Minas, D. Carnelli, E. Tervoort, A.R. Studart, 3D Printing of emulsions and foams into hierarchical porous ceramics, Adv. Mater. 28 (2016) 9993-99. https://doi.org/10.1002/adma.201603390.
[34] M.R. Sommer, L. Alison, C. Minas, E. Tervoort, P.A. Rühs, A.R. Studart, 3D printing of concentrated emulsions into multiphase biocompatible soft materials, Soft Matter, 13 (2017) 1794-1803. Doi: 10.1039/C6SM02682F.
[35] E. García-Tuñon, G. Machado, M. Schneider, S. Barg, R.V. Belld, E. Saiz, Complex ceramic architectures by directed assembly of 'responsive' particles, J. Eur. Ceram. Soc. 37 (2017) 199–211. https://doi.org/10.1016/j.jeurceramsoc.2016.06.050.
[36]. G. Turnbull, J. Clarke, F. Picard, P. Riches, L. Jia, F. Han, B. Li, W. Shu, 3D bioactive composite scaffolds for bone tissue engineering, Bioact. Mater. 3 (2018) 278-314. https://doi.org/10.1016/j.bioactmat.2017.10.001.
[37]. Y. Wen, S. Xun, M. Haoye, S. Baichuan, C. Peng, L. Xuejian, Z. Kaihong, Y. Xuan, P. Jiang, L. Shibi, 3D printed porous ceramic scaffolds for bone tissue engineering: a review, Biomater. Sci. 5 (2017) 1690-98. Doi:10.1039/c7bm00315c.
[38] W.E. Lee, G.P. Souza, C.J. McConville, T. Tarvornpanich, Y. Iqbal, Mullite formation in clays and clay-derived vitreous ceramics, J. Eur. Ceram. Soc. 28 (2008) 465-471. https://doi.org/10.1016/j.jeurceramsoc.2007.03.009.
[39]. Y. Jung, J.J. Li, H. Zreiqat, Doped calcium silicate ceramics: A new class of candidates for synthetic bone substitutes, Materials. 10 (2017) 153. https://doi.org/10.3390/ma10020153.

Figure captions

Fig.1 Details of scaffolds from H44-photocurable acrylic resin blend, fired in nitrogen: a-c) cubic-cell sample; c,d) diamond-cell sample

Fig.2 Details of scaffolds from H62C-photocurable acrylic resin blend, fired in nitrogen: a,b) cubic-cell sample; c) diamond-cell scaffold

Fig.3 Mineralogical comparison of samples from silicone-photocurable acrylic resin-reactive fillers blends, fired in air (at 1100°C), based on: a) H62C; b) H44

Fig. 4 Microstructural details of samples containing anhydrous borax (1.5 wt% $Na_2B_4O_7$ addition): a) macro-cracks in cubic-cell scaffold; b) defect within a strut of a diamond-cell scaffold; c) microporous structure of struts

Fig. 5 Microstructural details of cubic-cell scaffolds from hydrated borax (a: 1.5 wt% $Na_2B_4O_7$ addition; b: 3 wt%; c: 4.5 wt%)

Fig. 6 Mineralogical analysis of scaffolds fired at 1100oC from H44-based mixture added with hydrated borax: (a: 1.5 wt% $Na_2B_4O_7$ addition; b: 3 wt%; c: 4.5 wt%)

Fig.7 Microstructural details of H44-derived diamond-cell samples: a) 1.5 wt% $Na_2B_4O_7$ addition; b) 3 wt%; c,d) 4.5 wt%)

Fig 1

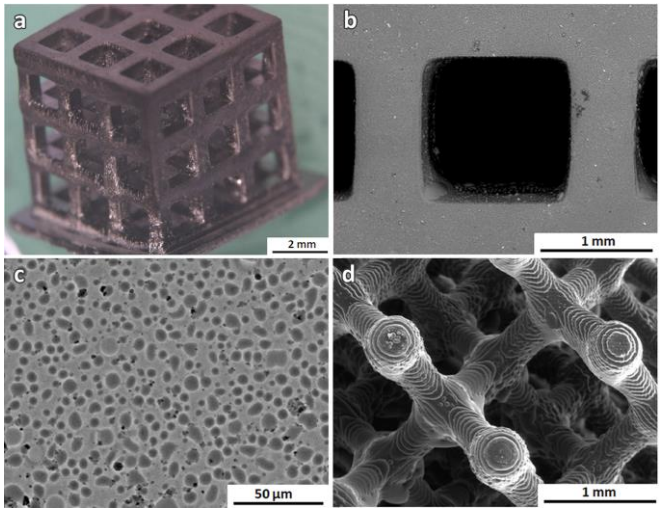

Fig 2

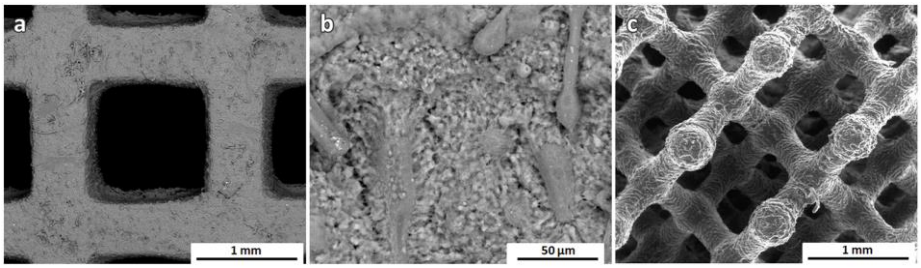

Fig 3

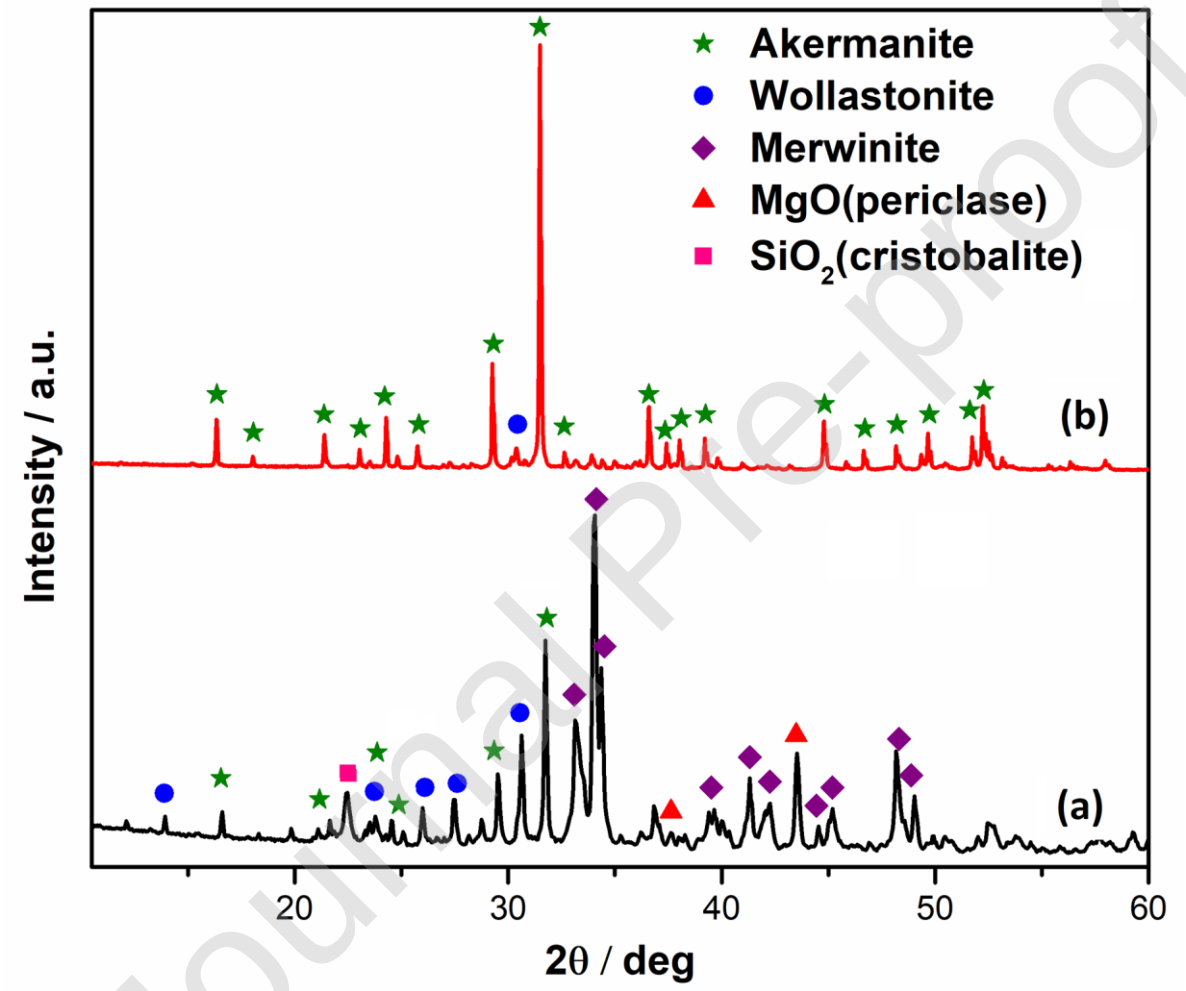

Fig 4

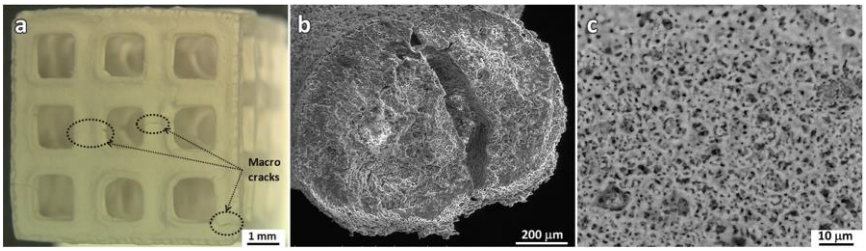

Fig 5

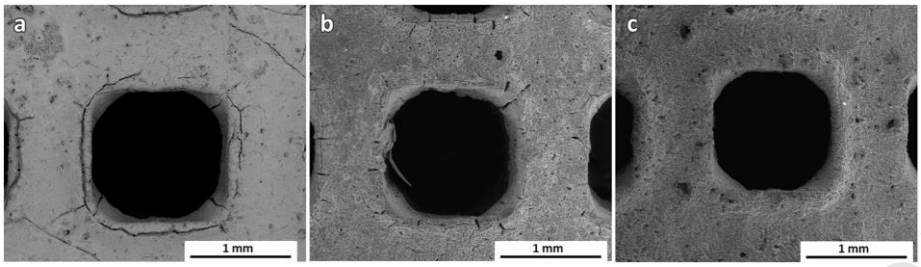

Fig 6

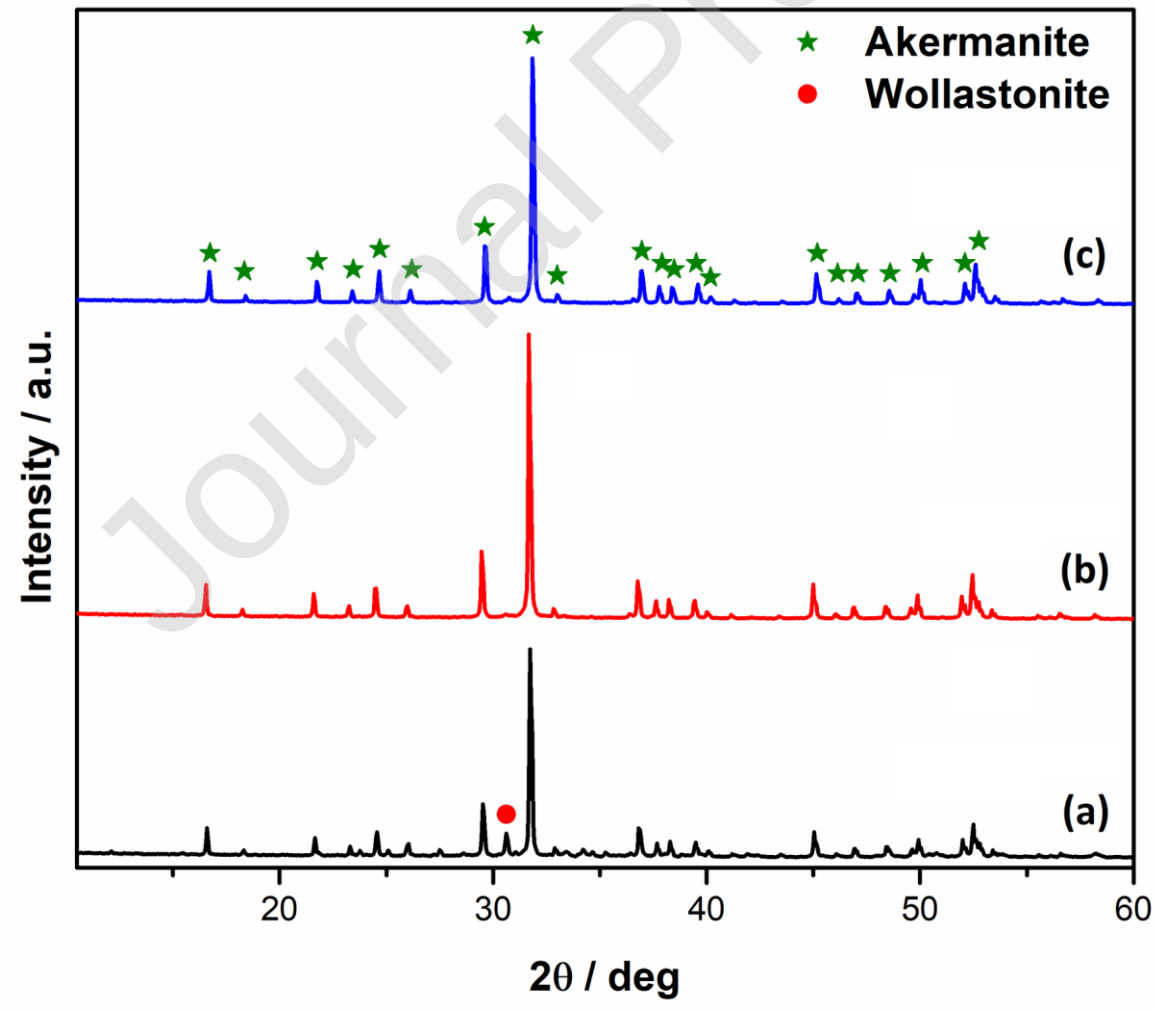

Fig 7

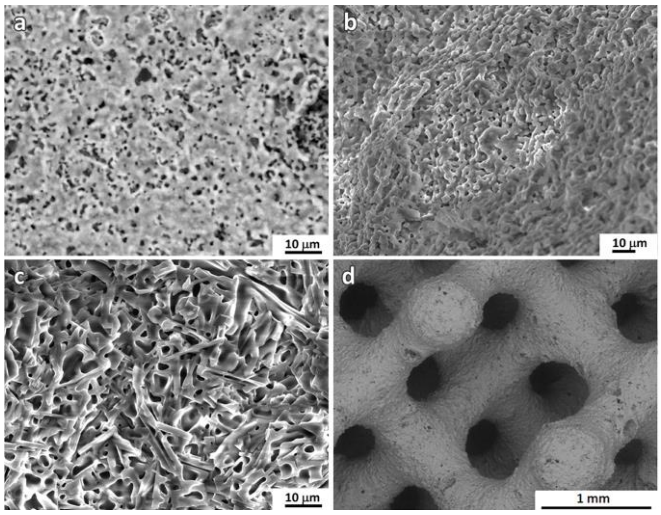

Table captions

Table 1 Physical and mechanical properties of SiOC scaffolds

Table 2 Physical and mechanical properties of åkermanite scaffolds from H44-based mixtures

Tables

3D SiOC structures		Geometrical density, ρ (g/cm^3)	Total porosity (vol %) [ρ_{rel}=1-P_{tot}]	Open porosity (vol %)	Compressive strength, σ_c (MPa) [σ_{bend} (MPa)]
H44	cubic	0.75 ± 0.02	62 ± 1 [0.38]	58 ± 1	24 ± 3
	diamond	0.35 ± 0.01	82 ± 1 [0.18]	79 ± 1	3 ± 0.3 [~208]
H62C	cubic	0.73 ± 0.01	64 ± 1 [0.36]	59 ± 1	21 ± 1
	diamond	0.27 ± 0.02	86 ± 1 [0.14]	84 ± 1	2 ± 0.5 [~206]

Table 1

$Na_2B_4O_7$ addition, by means of hydrated borax (wt%)	Design	Geometrical density, ρ (g/cm^3)	Total porosity (vol %) [ρ_{rel}=1-P_{tot}]	Open porosity (vol %)	Compressive strength, σ_c (MPa) [σ_{bend} (MPa)]
1.5	cubic	0.75 ± 0.05	74.1 ± 1.6 [0.26]	73.8 ± 1.6	1.5 ± 0.5
	diamond	0.27 ± 0.03	90.7 ± 1.0 [0.09]	90.6 ± 1.0	0.07 ± 0.01 [~12]
3	cubic	0.82 ± 0.03	72 .0 ± 1.0 [0.28]	71.5 ± 1	2.1 ± 0.3
	diamond	0.32 ± 0.01	89.0 ± 0.6 [0.11]	88.4 ± 0.7	0.25 ± 0.05 [~34]
4.5	cubic	0.98 ± 0.04	66.4 ± 1.3 [0.34]	65.3 ± 1.3	2.8 ± 0.4
	diamond	0.33 ± 0.03	88.6 ± 1.0 [0.11]	88.2 ± 1.0	0.40 ± 0.05 [~50]

Table 2